

# **Energy Management Control of a Hybrid Electric Vehicle with Two-Mode Electrically Variable Transmission**

Brian Bole<sup>1</sup>, Samuel Coogan<sup>2</sup>, Carlos Cubero-Ponce<sup>1</sup>, Derek Edwards<sup>1</sup>, Ryan Melsert<sup>1</sup>,  
David Taylor<sup>1</sup>

<sup>1</sup>*Georgia Institute of Technology, Atlanta, GA, 30332, USA.*

<sup>2</sup>*University of California, Berkeley, Berkeley, CA, 94720, USA.*

---

## **Abstract**

A hybrid electric vehicle with a two-mode continuously variable transmission and four fixed gear operating modes is modeled to enable a comparative investigation of the charge sustaining energy management control problem. Control strategies are designed using three distinct approaches: (1) explicit operating logic is defined in terms of comparison threshold values that can be tuned, using heuristic reasoning and/or model-based calculations, to operate the engine efficiently; (2) a static optimization, applied at each time instant, is used to minimize some measure of equivalent fuel consumption for the corresponding sequence of time instants; (3) a dynamic optimization, applied just once over the appropriate time interval, is used to minimize the actual fuel consumption over a drive cycle. The first approach requires only limited modeling information, and thus has the benefit of quick and simple programming. The second approach is based on optimization so as to directly exploit available modeling information. The third approach will find the vehicle control for optimal fuel efficiency, but it does not lead to an implementable strategy since prior knowledge of the drive cycle is required.

*Keywords: power-split hybrid, energy management control, equivalent fuel optimization, dynamic programming*

---

## **1 Introduction**

The powertrain architecture selected for this investigation is a type of power-split architecture. Power-split architectures provide both a direct mechanical power path and an electromechanical power path between the internal combustion engine and the wheels. This design combines the advantages of single-path architectures such as parallel (mechanical only) and series (electromechanical only) architectures.

A simply-gearred mechanical path is highly efficient, i.e. approximately 95% of the power provided by the engine can be transmitted to the wheels through such a path; however, the engine speed is constrained by just a few fixed gear ratios, leading to potentially inefficient engine operation. An electromechanical path allows only about 75% of engine

power to reach the wheels due to the double conversion of power through a generator and a motor; however, the resulting decoupling of the engine and the wheels can be exploited to ensure efficient operation of the engine. A well-known example of the combined-path power-split architecture is employed in the Toyota Prius hybrid electric vehicle (HEV), in which one planetary gearset and two electric machines are used to implement a one-mode electrically variable transmission (EVT). The particular type of power-split architecture considered in this publication is a two-mode EVT with the optional capability to operate as a purely mechanical transmission having four fixed gear ratios. This technology was developed by GM, beginning with a patent on the first EVT architecture with two modes [1], evolving to a patent on the first EVT architecture with both an

input-split mode and a compound-split mode featuring planetary gearsets of both the single-planet type and double-planet type [2], and culminating with a patent on the first EVT architecture as just described to be extended with four fixed gear ratios [3].

Two-mode EVTs can be designed to operate more efficiently than one-mode EVTs, due to the existence of additional “mechanical points,” i.e. operating points at which the electromechanical path carries no power, as explained in several recent publications that compare recently introduced two-mode architectures with the one-mode EVT employed in the market-leading Toyota Prius THS-II [4, 5, 6]. A presentation of improvements in powertrain performance and efficiency that are enabled by adding the capacity for switching between fixed gear and power-split powertrain operation is given in [7]. A description of the front-wheel-drive (FWD) GM two-mode input-split compound-split EVT with four fixed ratios can be found in [8]. Mathematical modeling of the powertrain architecture disclosed in [8], i.e. the world’s first front-wheel-drive two-mode hybrid transaxle architecture appears in [9, 10]. The authors of [9] simulate an equivalent fuel consumption minimization energy management control strategy on a FWD THS-II one-mode HEV and a FWD GM two-mode HEV in order to analyze the behavior of the energy management controller as it operates on each these powertrain architectures over a drive cycle. This paper uses similar vehicle modeling to that presented in [9], to explore the comparative effect that four distinct types of energy management control strategies have on overall vehicle fuel economy and the instantaneous operating modes chosen for powertrain components within a simulated FWD GM two-mode HEV over a particular mandated drive cycle.

## 2 Speed and Torque Constraints

A stick diagram of the hybrid transmission considered in this paper is shown in Fig. 1. There are two planetary gearsets denoted  $PG_1$  and  $PG_2$ , two motor-generator units denoted  $MG_a$  and  $MG_b$ , two braking clutches denoted  $C_1$  and  $C_4$ , and two rotating clutches denoted  $C_2$  and  $C_3$ . Power is received through the external input which is continuously connected to the ring gear of  $PG_1$ , and power is transmitted through the external output which is continuously connected to the carrier of  $PG_2$ . Internally,  $PG_1$  and  $PG_2$  are continuously connected to each other,  $MG_a$  is continuously connected to  $PG_1$ , and  $MG_b$  is con-

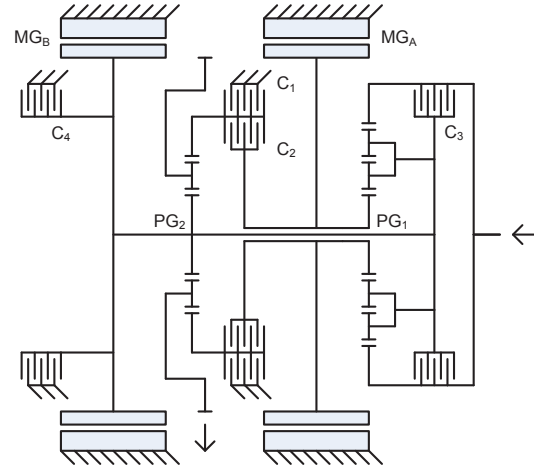


Figure 1: Stick diagram of two-mode EVT with four fixed-gear ratios.

Table 1: Clutch Table for Mode Selection

Mode	$M$	$C_1$	$C_2$	$C_3$	$C_4$
EVT-1	1	on			
EVT-2	2		on		
FG-1	3	on		on	
FG-2	4	on	on		
FG-3	5		on	on	
FG-4	6		on		on

tinuously connected to both  $PG_1$  and  $PG_2$ . The four clutches allow additional connections to be made selectively, in order to impose the operating modes indicated in Table 1. The external output is a centrally located transfer gear rather than a longitudinally oriented drive shaft, since this transmission is part of a transaxle assembly for a front-engine, front-wheel-drive vehicle.

The interconnections indicated in Fig. 1 and Table 1 lead to transmission constraint equations that must be derived separately for each mode of operation. The speed and torque at the output ( $\omega_o, T_o$ ) are dictated by driver demand, whereas the speeds and torques at the input ( $\omega_i, T_i$ ) and at the motor-generator units ( $\omega_a, T_a$ ) and ( $\omega_b, T_b$ ) are not all predetermined; design freedoms vary with mode selection.

As shown in Fig. 1, the transmission considered here is composed of two distinct types of planetary gearsets. For either type, modeling equations are derived using the following concepts. Kinematic speed constraints are derived by enforcing speed agreement at points where gear meshing occurs; carrier speed  $\omega_c$ , ring gear speed  $\omega_r$  and sun gear speed  $\omega_s$  are assumed positive for a common direction (e.g. all speeds directed clockwise). Dynamic torque con-

straints are derived by imposing a power balance, and these reduce to steady-state torque constraints if accelerations are neglected; carrier torque  $T_c$ , ring gear torque  $T_r$  and sun gear torque  $T_s$  are assumed positive for a common direction (e.g. all torques directed inward).

The first planetary gearset is of the double-planet type. The kinematic speed constraint is

$$\omega_{c1} = \frac{1}{1 - \rho_1} \omega_{r1} - \frac{\rho_1}{1 - \rho_1} \omega_{s1} \quad (1)$$

and the steady-state torque constraints are

$$-T_{c1} = (1 - \rho_1) T_{r1} = \frac{1 - \rho_1}{-\rho_1} T_{s1} \quad (2)$$

if losses are neglected. Both relations are characterized by the ratio of sun gear teeth to ring gear teeth,  $\rho_1 = n_{s1}/n_{r1}$ .

The second planetary gearset is of the single-planet type. The kinematic speed constraint is

$$\omega_{c2} = \frac{1}{1 + \rho_2} \omega_{r2} + \frac{\rho_2}{1 + \rho_2} \omega_{s2} \quad (3)$$

and the steady-state torque constraints are

$$-T_{c2} = (1 + \rho_2) T_{r2} = \frac{1 + \rho_2}{\rho_2} T_{s2} \quad (4)$$

if losses are neglected. Both relations are characterized by the ratio of sun gear teeth to ring gear teeth,  $\rho_2 = n_{s2}/n_{r2}$ .

Two relevant facts regarding planetary gearsets are: if any two terminals are connected together, then all three terminals will rotate at the same speed in the same direction, i.e. the gearset becomes locked-up; if any one terminal is held stationary, then no power flows through that terminal, i.e. the gearset reduces to a conventional two-terminal gearset. The speeds of planet gears internal to the planetary gearsets are not expressed directly in the kinematic equations presented in this publication; however, the maximum allowable rotation speeds of these gears will impose limitations on the maximum allowable speed ratio between any two terminals of the planetary gearset, as described in [10].

## 2.1 Variable-Ratio Operating Modes

For the transmission modeling equations presented here, the positive directions for mechanical power flow are taken to be into the input terminal, out of the output terminal, and out of both motor-generators.

In the EVT modes, a fraction of the input power can be diverted to an electromechanical path, so it is possible to choose  $(\omega_i, T_i)$  independently from  $(\omega_o, T_o)$ . Setpoints for  $MG_a$  and  $MG_b$  are implemented by imbedded speed controllers to enable the desired input-output decoupling.

### 2.1.1 EVT-1

This is an input-split mode, achieved by holding the ring gear of  $PG_2$  stationary. The input power is split by  $PG_1$  whereas  $PG_2$  serves as a conventional two-terminal gearset. Using (1) and (3) with  $\omega_{s2} = \omega_{c1}$  and  $\omega_{r2} = 0$ , the speed constraints are

$$\omega_a = \frac{1}{\rho_1} \omega_i - \frac{(1 - \rho_1)(1 + \rho_2)}{\rho_1 \rho_2} \omega_o \quad (5)$$

$$\omega_b = \frac{1 + \rho_2}{\rho_2} \omega_o \quad (6)$$

and using (2) and (4) the steady-state torque constraints are

$$T_a = -\rho_1 T_i \quad (7)$$

$$T_b = -(1 - \rho_1) T_i + \frac{\rho_2}{1 + \rho_2} T_o \quad (8)$$

From (5)–(6), there are two speed ratios at which one of the electric machines does not rotate, and they are determined from  $\rho_1$  and  $\rho_2$  according to

$$\frac{\omega_o}{\omega_i} = \begin{cases} 0 & , \omega_b = 0 \\ \frac{\rho_2}{(1 - \rho_1)(1 + \rho_2)} & , \omega_a = 0 \end{cases} \quad (9)$$

These speed ratios are called mechanical points because they correspond to power taking a direct mechanical path to the output instead of being partially diverted to the electromechanical path by one of the electric machines.

### 2.1.2 EVT-2

This is a compound-split mode, achieved by locking the ring gear of  $PG_2$  to the sun gear of  $PG_1$ . The input power is split twice, by  $PG_1$  at the input and by  $PG_2$  at the output. Using (1) and (3) with  $\omega_{s2} = \omega_{c1}$  and  $\omega_{r2} = \omega_{s1}$ , the speed constraints are

$$\omega_a = \frac{-\rho_2 \omega_i}{1 - \rho_1 - \rho_1 \rho_2} + \frac{(1 - \rho_1)(1 + \rho_2)}{1 - \rho_1 - \rho_1 \rho_2} \omega_o \quad (10)$$

$$\omega_b = \frac{1}{1 - \rho_1 - \rho_1 \rho_2} \omega_i - \frac{\rho_1(1 + \rho_2)}{1 - \rho_1 - \rho_1 \rho_2} \omega_o \quad (11)$$

and using (2) and (4) the steady-state torque constraints are

$$T_a = -\rho_1 T_i + \frac{1}{1+\rho_2} T_o \quad (12)$$

$$T_b = -(1-\rho_1)T_i + \frac{\rho_2}{1+\rho_2} T_o \quad (13)$$

From (10)–(11), there are two speed ratios at which one of the electric machines does not rotate, and they are determined from  $\rho_1$  and  $\rho_2$  according to

$$\frac{\omega_o}{\omega_i} = \begin{cases} \frac{\rho_2}{(1-\rho_1)(1+\rho_2)} & , \omega_a = 0 \\ \frac{1}{\rho_1(1+\rho_2)} & , \omega_b = 0 \end{cases} \quad (14)$$

These speed ratios are called mechanical points for the same reason stated above; note that both variable-ratio modes share a common mechanical point.

## 2.2 Fixed-Ratio Operating Modes

As indicated in Fig. 1 and Table 1, fixed-ratio modes are also available. Their inclusion enables engine power to be transmitted mechanically to the output, without the necessity of power flow through the electromechanical path; this permits use of electric machines with lower power ratings. By disabling the less-efficient electromechanical path, fixed-ratio operation also provides lower fuel consumption if the engine operating point is near optimum. Moreover, if desired, the electric machines can also be used to provide additional output power in fixed-ratio modes.

### 2.2.1 FG-1

Using (1) and (3) with  $\omega_{s_2} = \omega_{c_1} = \omega_{r_1}$  and  $\omega_{r_2} = 0$ , the speed constraints are

$$\omega_i = \omega_a = \omega_b = \frac{1+\rho_2}{\rho_2} \omega_o \quad (15)$$

From (2) and (4) the steady-state torque constraint is

$$T_o = \frac{1+\rho_2}{\rho_2} (T_i + T_a + T_b) \quad (16)$$

### 2.2.2 FG-2

Using (1) and (3) with  $\omega_{s_2} = \omega_{c_1}$  and  $\omega_{r_2} = \omega_{s_1} = 0$ , the speed constraints are

$$\omega_i = \frac{(1-\rho_1)(1+\rho_2)}{\rho_2} \omega_o \quad (17)$$

$$\omega_a = 0, \omega_b = \frac{1+\rho_2}{\rho_2} \omega_o \quad (18)$$

From (2) and (4) the steady-state torque constraint is

$$T_o = \frac{(1-\rho_1)(1+\rho_2)}{\rho_2} T_i + \frac{1+\rho_2}{\rho_2} T_b \quad (19)$$

The speed ratio of this mode matches the boundary between the normal ranges of EVT-1 and EVT-2 operation. Since  $MG_a$  does not rotate, it should not be energized.

### 2.2.3 FG-3

Using (1) and (3) with  $\omega_{s_2} = \omega_{c_1} = \omega_{r_1}$  and  $\omega_{r_2} = \omega_{s_1}$ , the speed constraint is

$$\omega_i = \omega_a = \omega_b = \omega_o \quad (20)$$

From (2) and (4) the steady-state torque constraint is

$$T_o = T_i + T_a + T_b \quad (21)$$

### 2.2.4 FG-4

Using (1) and (3) with  $\omega_{s_2} = \omega_{c_1} = 0$  and  $\omega_{r_2} = \omega_{s_1}$ , the speed constraints are

$$\omega_i = \rho_1(1+\rho_2)\omega_o \quad (22)$$

$$\omega_a = (1+\rho_2)\omega_o, \omega_b = 0 \quad (23)$$

From (2) and (4) the steady-state torque constraint is

$$T_o = \rho_1(1+\rho_2)T_i + (1+\rho_2)T_a \quad (24)$$

Since  $MG_b$  does not rotate in this mode, it should not be energized.

## 3 Power Flow Analysis

### 3.1 Variable-Ratio Operating Modes

The idealized case of lossless power transmission for propulsion with zero battery power is briefly considered in order to illuminate the role of the electric machines in the EVT modes, and to identify operating conditions that should be avoided. Fig. 1 is redrawn as shown in Fig. 2 to more clearly illustrate the power flow paths as well as the preferred directions for power flow.

Operating speeds at  $PG_1$ ,  $PG_2$ ,  $MG_a$  and  $MG_b$  are all computed using (5)–(6) in EVT-1 or (10)–(11) in EVT-2. Torque splits at  $PG_1$  and  $PG_2$  are computed using (2) and (4), respectively, whereas the torque splits at  $MG_a$  and  $MG_b$  are computed using (7)–(8) in EVT-1 or (12)–(13) in EVT-2. Following this procedure, the fraction of input power flowing through each branch of Fig. 2 may be expressed as an explicit function of the ratio of output speed to input speed.

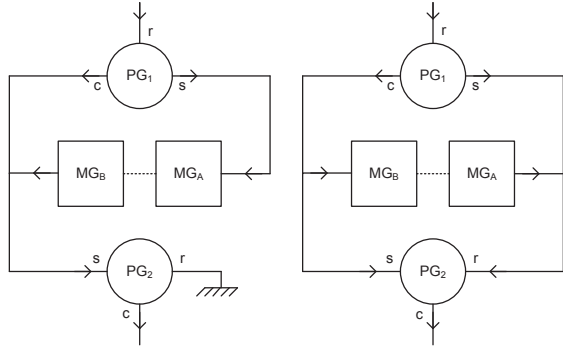


Figure 2: Preferred propulsive power directions (left = EVT-1, right = EVT-2).

EVT-1:

$$\frac{P_a}{P_i} = -1 + \frac{(1 - \rho_1)(1 + \rho_2)}{\rho_2} \frac{\omega_o}{\omega_i} \quad (25)$$

$$\frac{P_b}{P_i} = \frac{P_o}{P_i} - \frac{(1 - \rho_1)(1 + \rho_2)}{\rho_2} \frac{\omega_o}{\omega_i} \quad (26)$$

EVT-2:

$$\frac{P_a}{P_i} = c_1 - \frac{1}{2} + c_2 \frac{\omega_o}{\omega_i} + \left( \frac{1}{2} + c_3 + c_4 \frac{\omega_i}{\omega_o} \right) \frac{P_o}{P_i} \quad (27)$$

$$\frac{P_b}{P_i} = \frac{\omega_o}{\omega_i} - \frac{1}{2} - c_1 - c_2 + \left( \frac{1}{2} - c_3 - c_4 \frac{\omega_i}{\omega_o} \right) \frac{P_o}{P_i} \quad (28)$$

Normalized power flow is shown as a function of input-output speed ratio in Fig. 3, where the sign convention for power flow direction is defined in Fig. 2. The values of  $\rho_1$  and  $\rho_2$  used in Fig. 3 are listed in Table 3; the black circles correspond to the mechanical points defined by (9) and (14). Inspection of Figs. 2 and 3 reveals the possibility of undesired circulating power loops, which require planetary gearsets to support power levels exceeding the applied input power.

*Case 1:* All speed ratios in the range

$$0 < \frac{\omega_o}{\omega_i} < \frac{\rho_2}{(1 - \rho_1)(1 + \rho_2)} \quad (29)$$

result in preferred power flow directions for EVT-1, but circulating power loops on the lower mesh and the outer mesh for EVT-2. For this reason, EVT-1 is generally the preferred variable-ratio mode within this speed ratio range.

*Case 2:* All speed ratios in the range

$$\frac{\rho_2}{(1 - \rho_1)(1 + \rho_2)} < \frac{\omega_o}{\omega_i} < \frac{1}{\rho_1(1 + \rho_2)} \quad (30)$$

result in preferred power flow directions for EVT-2, but a circulating power loop on the upper mesh

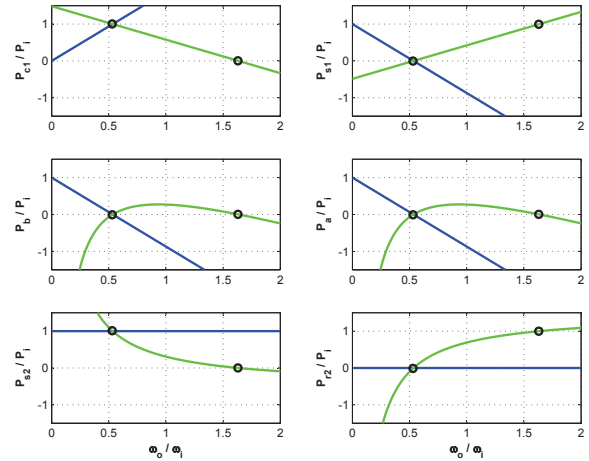


Figure 3: Normalized propulsive power values (blue = EVT-1, green = EVT-2).

for EVT-1. For this reason, EVT-2 is generally the preferred variable-ratio mode within this speed ratio range.

*Case 3:* All speed ratios in the range

$$\frac{1}{\rho_1(1 + \rho_2)} < \frac{\omega_o}{\omega_i} < \infty \quad (31)$$

result in a circulating power loop on the upper mesh for EVT-1 and circulating power loops on the upper mesh and the outer mesh for EVT-2. For this reason, this speed ratio range should generally be avoided when using variable-ratio modes.

Following this logic for propulsion with constant engine speed, vehicle launch would occur in EVT-1 with all the engine power flowing through the electromechanical path, with  $MG_a$  generating and  $MG_b$  motoring. As the vehicle speed increases, the engine power flowing through the electromechanical path would decrease until it reaches zero at the mechanical point shared by EVT-1 and EVT-2. At this point, whether in EVT-1 or EVT-2, no power flows through the electromechanical path or through the ring gear of  $PG_2$  and, consequently, a smooth shift from EVT-1 to EVT-2 is made possible. As the vehicle speed increases up to the second mechanical point of EVT-2, now with  $MG_b$  generating and  $MG_a$  motoring, the percent engine power flowing through the electromechanical path increases from zero up to a peak value of 27.2% and then decreases back to zero.

## 4 Energy Management Control

### 4.1 Problem Formulation

The purpose of the transmission is to provide a demanded output torque  $T_o$  at a given output speed  $\omega_o$ , within limits. The required output power  $T_o\omega_o$  may be derived from engine power  $T_i\omega_i$  and/or from battery power  $P_b$ , both of which are magnitude limited. The battery is an energy buffer that is not recharged by external means, so the battery state of charge (SOC)  $x$  must be maintained within acceptable limits at all times. Any recharging of the battery takes place on-board by operating one or both electric machines as generators. The only sources of mechanical energy for on-board recharging are: the kinetic and potential energies recovered from the vehicle's mass during braking, and the thermal energy released within the engine by the fuel combustion process.

The energy management controller is responsible for selecting a transmission operating mode  $M$ , the engine-fuel on/off status  $E$ , battery power  $P_b$ , and any speeds and torques that are free to assign to the engine and electric machines for the selected mode. Ideally, these selections would be made so as to satisfy driver power demands, maintain battery state of charge, and minimize fuel consumption and emissions. The sensor signals that could be used in the selection process include: vehicle speed, accelerator and brake pedal positions, and battery SOC.

Fixed-gear modes afford the energy management controller degrees of freedom in the selection of engine and electric machine torques that may be exploited to efficiently meet a given driver demanded output torque, which is interpreted from the gas and brake pedal positions. The EVT modes will afford the energy management controller even more degrees of freedom; in this case, both engine torque and speed can be selected without regard to the output torque-speed operating point, since the electric machines can then be operated to impose the desired operating point.

Energy usage within the vehicle's powertrain will always be greater than propulsive energy delivered to the vehicle's wheels, due to inefficiencies associated with the instantaneous power conversions occurring within the powertrain's components. The thermal efficiency of the internal combustion engine, the power efficiency of the electric machines, and the electrical energy loss that is associated with sinking and sourcing power from the battery, are each dependent on the manner in which the energy management controller selects from available operational degrees of freedom

at each instant on a given drive cycle.

The thermal efficiency of the engine is denoted

$$\eta_i(T_i, \omega_i) = \frac{T_i\omega_i}{H_l\dot{m}_f} \quad (32)$$

where  $H_l$  denotes the lower heating value of the fuel and  $\dot{m}_f$  denotes the mass flow rate of the fuel.

The electric machines and their power electronic converters are characterized by their power efficiencies

$$\eta_*(T_*, \omega_*) = \begin{cases} \frac{T_*\omega_*}{P_{e,*}} & , T_*\omega_* > 0 \\ \frac{P_{e,*}}{T_*\omega_*} & , T_*\omega_* < 0 \end{cases} \quad * = a \text{ or } b \quad (33)$$

where  $P_{e,*}$  denotes the electrical power flowing into the power electronic converter of electric machine  $*$ .

Clutch-selectable interconnections within the transmission will determine specific constraints on feasible speeds and torques of powertrain components for each mode of operation, as has been described. On the basis of this type of transmission model, three approaches to energy management controller development are explored: heuristic control, real-time optimization-based control, and optimal control via dynamic programming.

### 4.2 Heuristic Control

A straightforward method for designing an energy management controller is to rely on explicit operating logic defined in terms of comparison threshold values. In this case, the threshold values are defined in an attempt to ensure efficient operation of the engine over a drive cycle, while keeping the battery SOC within specified upper and lower bounds; these threshold values may be tuned heuristically, or with the aid of modeling information.

The simplistic heuristic strategy explored in this publication makes heavy use of the EVT modes, which allow the engine operating point to be chosen independently of vehicle state. Because high efficiency operation of the engine corresponds to a higher output power than is typically needed by the driver, the heuristic strategy is designed to alternate between a charging mode, in which the engine is run at a high power (high efficiency) operating point, and a discharging mode, in which the engine is turned off or run at a lower power (lower efficiency) operating point. Switching from one mode to the other occurs when upper or lower SOC boundaries are reached.

Also, if the engine would be operated efficiently at any time in a fixed gear mode, with no electric assist, then that mode is chosen. This strategy is implemented by employing the rules listed in Fig. 4. The design parameters in this strategy are the low-power engine setpoint  $(T_{i_L}, \omega_{i_L})$  and the high-power engine setpoint  $(T_{i_H}, \omega_{i_H})$ , as well as the threshold values  $\eta_i^*$ ,  $v_{1/2}$ ,  $v_{\text{off}}$ ,  $x_{\text{min}}$ , and  $x_{\text{max}}$ , that are defined in Table 3. The variables  $v$  and  $x$  are used to represent vehicle speed and battery state of charge respectively;  $T_i^k$  and  $\omega_i^k$  are used to represent the engine torque and speed that would be required to produce a given commanded powertrain output torque and speed if the fixed gear ratio  $k$  were active.

Heuristic or fuzzy logic based controls are commonly used in industry and academic applications of hybrid vehicle controls [11, 12]. While heuristic controllers can provide an effective means of exploiting heuristic knowledge available to controls designers regarding efficient operation of the hybrid powertrain, it should be expected that optimization-based controls will result in significant improvements in overall efficiency, assuming the availability of sufficient vehicle modeling information and on-board computational power. In Section 5, the results obtained using the simplistic heuristic control strategy are contrasted with the comparatively more complex controls resulting from direct numerical optimization of a cost function at each control time-period.

### 4.3 Optimization-Based Control

The energy management control problem for maximizing the fuel efficiency of a charge sustaining vehicle can be expressed as the following constrained optimization problem:

$$\text{minimize } m_f(T) = \int_0^T \dot{m}_f(u, w) dt \quad (34)$$

$$\text{subject to } \dot{x} = f(x, u, w), x(0) \text{ given} \quad (35)$$

$$x_{\text{min}} \leq x \leq x_{\text{max}}, \text{ for } 0 \leq t \leq T \quad (36)$$

$$x(T) \approx x(0) \quad (37)$$

where the objective of this optimization problem is to minimize the mass of fuel  $m_f(T)$  consumed during a drive cycle of duration  $T$ . The drive cycle is characterized by the exogenous input  $w$ , which dictates a vehicle speed versus time requirement; or equivalently, if vehicle and physics are known, then  $w$  dictates the transmission output speed and torque required of the energy management controller at each time instant over a given drive cycle. The rate of fuel consumption at any time instant will depend on the nature of

*Criterion for fixed-ratio modes (engine only):*

set  $\delta_k = \eta_i(T_i^k, \omega_i^k) - \eta_i^*, k = 1, \dots, 4$

set  $\Delta = \max \{\delta_k : k = 1, \dots, 4\}$

if  $\Delta > 0$

select FG- $k$  such that  $\Delta = \delta_k$

else

select an EVT mode

end

*Criterion for variable-ratio modes (engine on/off):*

if  $v < v_{1/2}$

select EVT-1

else

select EVT-2

end

if charge\_discharge\_mode = discharge

if  $v < v_{\text{off}}$

turn engine off

else

operate engine at low power,  $(T_{i_L}, \omega_{i_L})$

end

else

operate engine at high power,  $(T_{i_H}, \omega_{i_H})$

end

*Battery operation mode:*

if  $x < x_{\text{min}}$

set: charge\_discharge\_mode = charge

else if  $x > x_{\text{max}}$

set: charge\_discharge\_mode = discharge

end

Figure 4: Heuristic control operating logic.

the drive cycle, through  $w$ , as well as on the control input  $u$ , which includes all choices to be made by the energy management controller. The battery's SOC satisfies a dynamic equation involving battery power, and hence is also influenced by  $w$  and  $u$ .

An inherent trade-off is evident in the optimization problem: over-reliance on engine power will unduly degrade the objective (34) but will allow the constraints, (36) and (37) to be more easily satisfied; on the other hand, generous use of battery power enhances the objective but cannot be sustained without violating the constraints. Solution of this problem is therefore non-trivial.

If driver desired performance were known from  $t_o$  to  $T$ , then the optimization problem expressed in (34)-(37) could be solved directly. The require-

ment of *a priori* knowledge means that a direct solution of (34)-(37) is generally non-causal and non-implementable in practice; however, computing the optimal control solution for certain reference drive cycles is useful for comparative purposes. Dynamic programming [13], linear programming [14], and optimal control theory [15] have been shown to generate solutions for the non-implementable optimal HEV control strategy. Implementable optimization approaches will be causal and real-time executable. At each control time-step the supervisory controller will minimize an engineered cost function, using only information regarding past operating conditions to estimate the best present powertrain set-points for a presently desired transmission torque-speed output. Section 4.4 discusses an optimal yet non-implementable approach to supervisory control and this section will introduce strategies for real-time implementable optimization-based controls.

The most common form of the real-time optimization-based control for charge sustaining parallel-hybrid vehicles is an equivalent-consumption minimization (ECM) strategy [16]. This strategy will select a single powertrain operating point at each time-instant from a range of feasible operating points by minimizing an instantaneous performance function,

$$P = P_f + sP_b \quad (38)$$

where  $P_f = H_f \dot{m}_f$  represents the instantaneous fuel power consumed by potential powertrain operating modes,  $P_b$  represents instantaneous battery power draw, and  $s$  is an equivalence factor used to equate the cost of instantaneous electrical power and fuel power consumption. Assuming that sufficient computational power is available to solve for the powertrain control that minimizes (38) at each control time-instant, then the performance of this type of energy management controller is determined solely by the manner in which the equivalence factor is specified.

Because all electrical energy consumed in a charge sustaining vehicle ultimately comes from burning fuel, the equivalence factor could be considered to have a “true” evaluation, which would exactly convert present electrical power consumption into an equivalent future liquid fuel consumption. Although, evaluation of this “true” equivalence factor is generally impossible in practice, due to the dependence of thermal, electrical, and mechanical energy exchanges on future driver inputs and future powertrain controls. In fact, if evaluation of the “true” equivalence factor was possible in practice, then minimization of (38) at each control time-step would be equivalent to a direct

minimization of the global optimization problem expressed in (34). Several recent publications on ECM have explored strategies for equivalence factor evaluation that attempt to approximate the “true” equivalence factor at a given control time-step using probabilistic estimation of future vehicle demands and corresponding future powertrain controls [17, 18].

The more typical approach to ECM, which is also utilized in this publication, does not explicitly incorporate modeling of future powertrain operation in the evaluation of an equivalence factor, but rather uses an equivalence factor that is based only on the present operating environment and the battery’s present SOC. In general, such ECM strategies will rely on empirical testing procedures to tune the parameters of an equivalence factor evaluation model. Ideally, the equivalence factor will result in an energy management controller that makes heavy use of the battery as an energy sink/source to enable efficient operation of all powertrain components at each control time-step, while also ensuring that battery SOC will always remain within specified upper and lower bounds. Publications on this topic vary widely in the methodology used to specify the equivalence factor; common strategies include: a constant value found experimentally [19], a function that varies the equivalence factor with battery SOC [20], and mixed strategies that use the current output speed and torque demanded of the drivetrain as well as SOC deviations to adjust the equivalence factor [21]. This publication explores two approaches for equivalence factor selection; the first approach represents a simplistic strategy in which the equivalence factor is varied as a linear function of battery SOC, and the second approach introduces a more complex, but more effective, mixed strategy, in which the equivalence factor is varied based on the efficiencies of presently available engine and electric machine operating points, as well as the present battery SOC.

#### 4.3.1 SOC-Based Equivalence Factor

This strategy updates the equivalence factor at each control time-instant using a piecewise linear function of SOC,

$$s = \begin{cases} s_{\max} & , x < x_{\min} \text{ and } P_b > 0 \\ s_{\min} & , x > x_{\max} \text{ and } P_b < 0 \\ mx + b & , \text{otherwise} \end{cases} \quad (39)$$

Observe that for  $m < 0$ , an increasing SOC will cause the equivalence factor to decrease, which will put more weight on fuel consumption minimization, resulting in higher electrical power consumption and

less energy storage in the battery; conversely, a decreasing SOC will result in higher fuel consumption and greater energy storage in the battery. Repeated simulations of the real-time energy management controls on a range of sample drive cycles were used to find values for  $m$  and  $b$  that resulted in high long-run fuel efficiencies, without violation of the battery SOC constraints. Boundary conditions were added to (39) to heavily penalize SOC excursions beyond the specified bounds; however, if  $m$  and  $b$  are chosen appropriately the battery SOC should rarely approach these bounds. The values of  $m$  and  $b$  used in the simulations described in Section 5 are given in Table 3.

#### 4.3.2 Adaptive Piecewise-Linear Equivalence Factor

After some tuning, the SOC-based linear equivalence factor can result in high fuel efficiencies and a charge sustaining behavior over a wide range of drive-cycles; however, more optimal results can be obtained by supplementing the linear dependence on SOC with additional linear dependencies on the powertrain and engine efficiencies corresponding to potential powertrain operating points. The improved strategy adjusts the parameters of (39) based on the engine thermal efficiency and electrical power transmission efficiencies of feasible powertrain operating points, using the following expressions:

$$\eta_e = \begin{cases} \frac{T_a \omega_a + T_b \omega_b}{P_{e,a} + P_{e,b} - P_{b,\text{loss}}} & , \text{ discharge} \\ \frac{P_{e,a} + P_{e,b} - P_{b,\text{loss}}}{T_a \omega_a + T_b \omega_b} & , \text{ charge} \end{cases} \quad (40)$$

$$\alpha = \frac{c_1(1 - \eta_i) + c_2(1 - \eta_e)}{P_b} \quad (41)$$

$$m = m' + \alpha \quad (42)$$

$$b = b' + \alpha \quad (43)$$

where  $P_{b,\text{loss}}$  denotes the electrical power dissipation within the battery,  $\eta_e$  represents the power efficiency of the combined the electrical path, which includes both electric machines and the battery, and  $c_1$ ,  $c_2$ ,  $m'$ , and  $b'$  are weighting coefficients found via repeated simulations on a variety of drive cycles. A discussion of parameter tuning for a similar ECM approach is given in [21]. The values of  $c_1$ ,  $c_2$ ,  $m'$ , and  $b'$  used in the simulations described in Section 5 are given in Table 3.

## 4.4 Optimal Control

To determine an upper bound on achievable performance, the solution of the optimal control problem given in (34)–(37) was approximated using dynamic programming. The constraints on  $x$ , given in (36), are enforced over a given drive-cycle, and an equality constraint is imposed on the initial and final values of battery SOC,  $x(T) = x(0)$ .

The dynamic programming implementation involves two steps. In the first step, an exhaustive search is performed in order to construct a table that identifies feasible values of

$$\{M, (T_i, \omega_i), (T_a, \omega_a), (T_b, \omega_b)\}$$

that minimize the instantaneous value of  $\dot{m}_f$  for a quantized set of  $(T_o, \omega_o, P_b)$ , where  $M$  represents the open or closed state of the transmission's clutches. By resolving this issue first, the number of choices remaining to completely specify the transmissions operating state at each time instant on a drive cycle is reduced to just the battery power. The only component of  $u$  that directly links to (35)–(37) is battery power, so it makes intuitive sense to first solve for all components of  $u$  that minimize  $\dot{m}_f$ , in terms of  $P_b$ , and then to manipulate  $P_b$  to minimize (34) using optimal control methods.

In the second step, the well-known dynamic programming method is employed to approximate the solution of optimal control problem. The table produced in the first step is leveraged to permit efficient computation of the optimizing time trajectory of battery power  $P_b$ , at which point all components of the transmission operating state are determined.

## 5 Simulation Results

Drive cycle simulation results are provided based on the standard model of road load, the transmission model of Section 2, the energy management controllers of Section 4, and the parameter values listed in Table 3. The engine and motor-generator units are modeled by their steady-state efficiency maps  $\eta_i(T_i, \omega_i)$ ,  $\eta_a(T_a, \omega_a)$  and  $\eta_b(T_b, \omega_b)$ .

The drive cycle is translated into  $(T_o, \omega_o)$  demands at one-second intervals. To facilitate comparisons, initial and final values of battery state of charge were forced to be nearly equal, meaning that the net energy used over the drive cycle is accurately represented by fuel consumption alone. This constraint is explicit in dynamic programming, but for the other control methods it was imposed through appropriate

Table 2: Fuel Consumption on UDDS Drive Cycle

Control Method	mpg
Heuristic	48
SOC-Based Equivalence Factor	48
Adaptive Piecewise-Linear Equivalence Factor	54
Non-Causal Dynamic Programming	56

Table 3: Numerical Values for Simulations

parameter	value	unit
mass	1746	kg
frontal area	2.642	m <sup>2</sup>
drag coefficient	0.386	
tire radius	0.352	m
final drive	3.29	
$(\rho_1, \rho_2)$	(44/104, 37/83)	
$E_b$	9.6	kWh
$(P_{b,min}, P_{b,max})$	(-50, 100)	kW
$(x_{min}, x_{max})$	(0.3, 0.7)	
$\eta_i^*$	0.3	
$(v_{1/2}, v_{off})$	(30, 30)	mph
$(T_{iL}, T_{iH})$	(20, 120)	Nm
$(\omega_{iL}, \omega_{iH})$	(900, 3000)	rpm
$(s_{min}, s_{max})$	(0, 10)	
$(m, b)$	$(-1.69, 3.46) \times 10^3$	
$(m', b')$	$(-1.33, 3.51) \times 10^3$	
$(c_1, c_2)$	$(26.6, 4.44) \times 10^3$	kW
$H_l$	44.4	MJ/kg

choice of the initial battery SOC. Since all of the controllers are forced to follow the drive cycle exactly, the energy required to move the vehicle is identical for each; the differences in the energy expended by each are due solely to differences in waste heat loss caused by inefficient operation of components.

Table 2 summarizes the miles-per-gallon (mpg) estimates obtained using the EPA urban dynamometer driving schedule (UDDS). The dynamic programming method results in the largest mpg estimate, as expected. The heuristic approach, which was designed to maximize engine operating efficiency, returns an impressive mpg estimate. The ECM strategy with an SOC-based equivalence factor returns the same mpg estimate as the heuristic approach, using a numerical method rather than expert rules. Finally, the adaptive equivalence factor used in the second ECM method gives an mpg estimate that is far superior to the other implementable methods.

Figure 6 shows engine operating points superimposed on the engine efficiency map and a histogram of the amount of time spent in each mode for each of the control strategies executed on the UDDS.

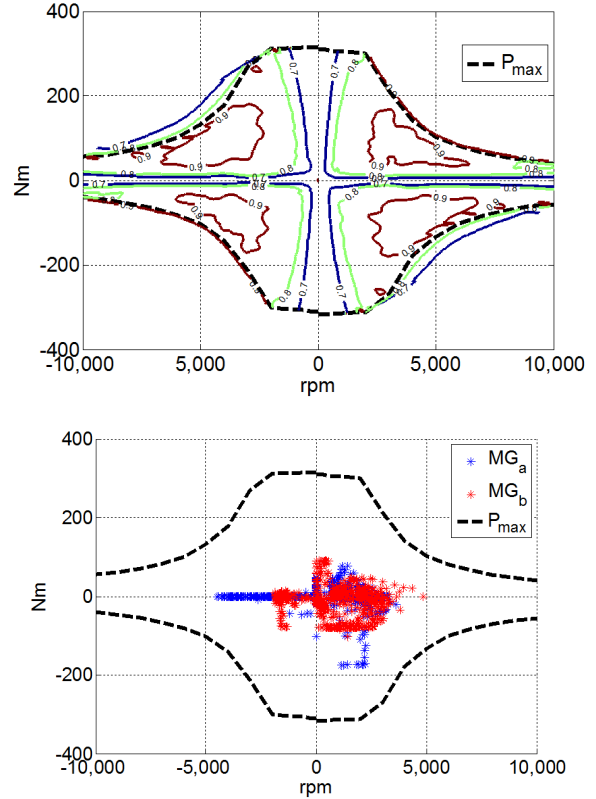
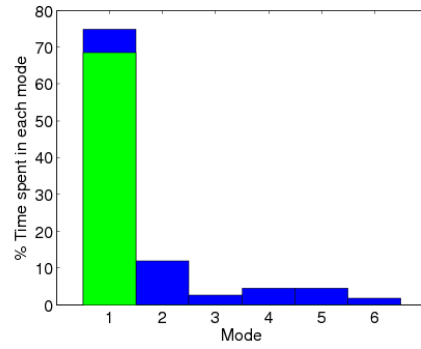
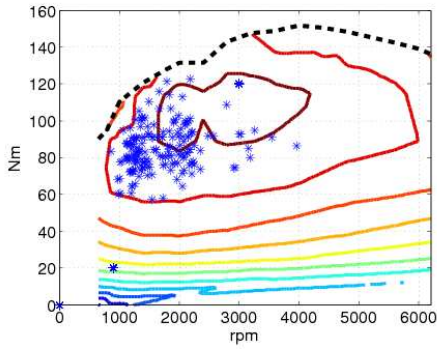


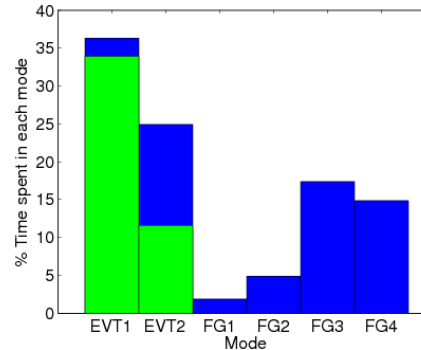
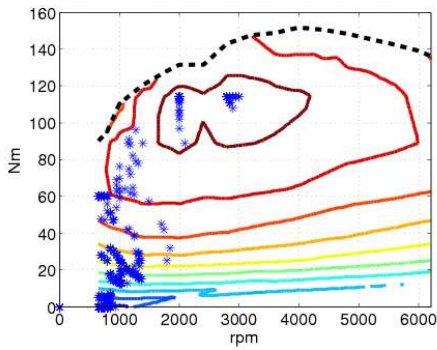
Figure 5: Electric machine efficiency map (top) and operating points dictated by dynamic programming for the UDDS.

Note that although the heuristic and piecewise-linear equivalence factor approaches both give the same mpg estimate, they control the engine and transmission much differently over the drive cycle. It would seem from the results that the heuristic strategy does the best job of optimizing engine efficiency on the drive cycle, even surpassing that of dynamic programming; however, this approach fails to account for inefficient operation of the electric machines and the battery. As can be seen from the optimization-based results, it is sometimes best to operate the engine inefficiently if that will facilitate a more efficient operation of the other components.

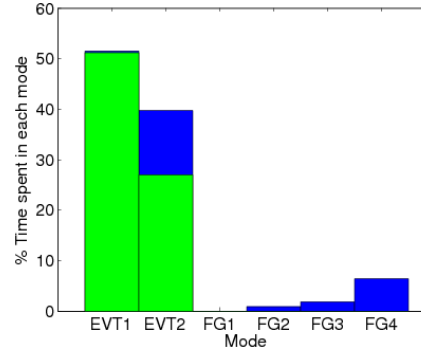
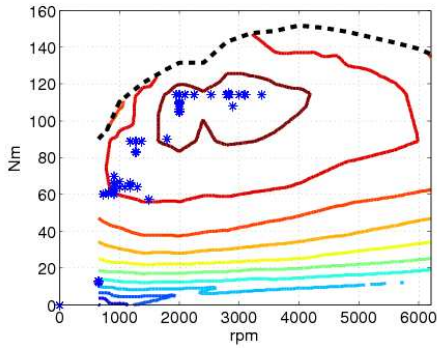
Figure 5 shows the operating points for  $MG_a$  and  $MG_b$  selected by dynamic programming on the UDDS. This figure shows that the optimal control operates the electric machines well within their power limits and, as with engine operation, it seems that it is sometimes best to operate the electric machines in lower efficiency regions in order to maximize the overall efficiency of the powertrain on the drive cycle.



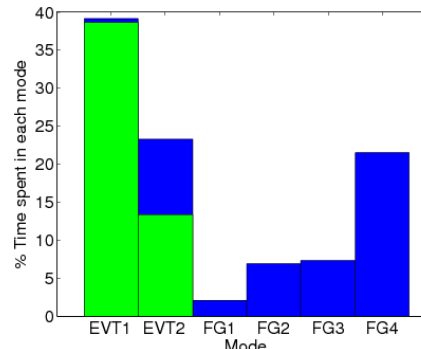
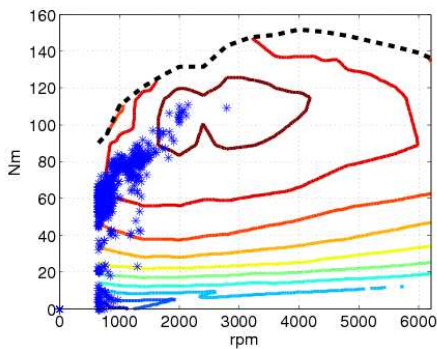
(a) Heuristic control.



(b) Optimization-based control using a piecewise-linear equivalence factor.



(c) Optimization-based control using an adaptive piecewise-linear equivalence factor.



(d) Optimal control using non-causal dynamic programming.

Figure 6: Comparative results for energy management methods on the UDDS. Left plots show engine operating points at each second of the drive cycle and right plots show the time spent in each mode; the green bars show the time spent with the engine off.

## 6 Conclusions

Heuristic, optimization-based, and optimal energy management control strategies were compared for the front-wheel-drive GM two-mode input-split compound-split EVT with four fixed ratios. Simulation results demonstrated that although the degrees of freedom available to the energy management controller could be used to largely avoid inefficient operation of the internal combustion engine or the transmission's electromechanical path at any particular time instant within a drive cycle, it is sometimes necessary to operate the components in lower efficiency regions in order to maximize the overall fuel economy of a charge sustaining HEV over a drive cycle.

The analysis presented in this paper omits some modeling details, such as mass factor and gearing inefficiencies which could significantly improve the accuracy and practicality of the developed control strategies. The control strategies described in this work are based upon static operating points that do not include the vehicle dynamics that come into play with changing vehicle speed, torque, or mode. Vehicle drivability, which includes handling and performance as interpreted by the driver were not considered. Also, accessory electrical loads such as those caused by air-conditioning, engine management, lighting, and multimedia among others were not included in the electrical load analysis.

## Acknowledgment

This work was supported by: EcoCAR Challenge, a three-year collegiate advanced vehicle technology engineering competition established by the Department of Energy and General Motors and managed by Argonne National Laboratory; and by the Department of Energy: Award Number DE-EE0002627.

## References

- [1] M. Schmidt, "Two-mode, input-split, parallel, hybrid transmission," US Patent 5,558,588, 1996.
- [2] A. Holmes, D. Klemen and M. Schmidt, "Electrically variable transmission with selective input split, compound split, neutral and reverse modes," US Patent 6,527,658, 2003.
- [3] A. Holmes, M. Schmidt, D. Klemen, J. Hendrickson and H. Sowul, "Electrically variable transmission with selective fixed ratio operation," US Patents 7,220,203 and 7,278,941, 2007.
- [4] J. Wishart, Y. Zhou and Z. Doug, "Review, modeling and simulation of two-mode hybrid vehicle architecture" *9th International Conference on Advanced Vehicle and Tire Technologies*, 2007.
- [5] B. Conlon, "Comparative analysis of single and combined hybrid electrically variable transmission operating modes," SAE Paper 2005-01-1162.
- [6] J. Meisel, "An Analytic Foundation for the Two-Mode Hybrid-Electric Powertrain with a Comparison to the Single-Mode Toyota Prius THS-II Powertrain" SAE 2009-01-1321
- [7] T. Grewe, B. Conlon and A. Holmes, "Defining the General Motors 2-Mode hybrid transmission," SAE Paper 2007-01-0273.
- [8] J. Hendrickson, A. Holmes and D. Freiman, "General Motors front wheel drive two-mode hybrid transmission," SAE Paper 2009-01-0508.
- [9] J. Arata, M. Leamy, J. Meisel, K. Cunefare and D. Taylor, "Backward-Looking Simulation of the Toyota Prius and General Motors Two-Mode Power-Split HEV Powertrains" SAE Paper: 2011-01-0948.
- [10] J. Meisel, "Kinematic study of the GM front-wheel drive two-mode transmission and the Toyota hybrid system THS-II transmission" SAE 2011-01-0876.
- [11] T. Moore and A. Lovins, "Vehicle design strategies to meet and exceed PHGV goals," *Proceedings on Electrical Hybrid Vehicle Implementation Technology*, pp. 79–121, 1995.
- [12] B. Mashadi and S. Emadi, "Dual-mode power-split transmission for hybrid electric vehicles," *IEEE Transactions on Vehicular Technology*, vol. 59, pp. 3223–3232, 2010.
- [13] A. Brahma, Y. Guezennec, and G. Rizzoni, "Optimal energy management in series hybrid electric vehicles," *Proceedings of the American Control Conference*, pp. 60–64, 2000.
- [14] E. Tate and S. Boyd, "Finding ultimate limits of performance for hybrid electric vehicles," *SAE 00FTT-50*, 1998.

- [15] P. Pisu and G. Rizzoni, "A comparative study of supervisory control strategies for hybrid electric vehicles," *IEEE Transactions on Control Systems Technology*, vol. 15, pp. 506–518, 2007.
- [16] A. Sciarretta and L. Guzzella, "Control of hybrid electric vehicles," *IEEE Control Systems Magazine*, vol. 27, pp. 60–70, 2007.
- [17] P. Rodatz, G. Paganelli, A. Sciarretta and L. Guzzella, "Optimal power management of an experimental fuel cell/supercapacitor-powered hybrid vehicle," *Control engineering practice*, vol. 13, pp. 41–53, 2005.
- [18] C. Musardo, G. Rizzoni, Y. Guezennec and B. Staccia, "A-ECMS: an adaptive algorithm for hybrid electric vehicle energy management," *European Journal of Control*, vol. 11, pp. 509–524, 2005.
- [19] K. Ahn and S. Cho, "Three types of simulation algorithms for evaluating the HEV fuel efficiency," *SAE 2007-01-1771*, 2007
- [20] J. Kessels, M. Koot, P. Bosch and D. Kok, "Online energy management for hybrid electric vehicles," *IEEE Transactions on Vehicular Technology*, vol. 57, pp. 3428–3440, 2008.
- [21] F. Salmasi, "Control strategies for hybrid electric vehicles: evolution, classification, comparison, and future trends," *IEEE Trans. on Vehicular Technology*, vol. 56, pp. 2393–2404, 2007.



Carlos Cubero-Ponce was a controls group leader for the Georgia Tech Eco-CAR team. He led the team's development of Hardware in Loop (HIL) and a supervisory control implementation on a DSpace controller. He is currently pursuing a Ph.D in Electrical Engineering at Georgia Tech.

Derek Edwards received his B.S. and M.S. degrees in Electrical and Computer Engineering from Georgia Tech in 2006 and 2009, respectively. He is currently pursuing his Ph.D. with an emphasis on intelligent transportation systems. His research focuses on optimal routing in passenger transportation systems. Specifically, his work seeks to provide demand-responsive public transportation options in low-density urban areas that are unsuited to traditional modes of transit.



Ryan Melsert graduated from Penn State University in 2004 with a B.S. in Mechanical Engineering and a B.S. in Engineering Science. He received an M.S. in Mechanical Engineering in 2007 and an MBA in 2010 from the Georgia Institute of Technology. His research at the Strategic Energy Institute focuses on developing innovative short-term high-impact solutions to our global energy challenges. Specifically, on the development of cellulosic biofuels, solar thermal power generation, hybrid-electric vehicle design, and thermal systems design.



David Taylor received his B.S. in Electrical Engineering from the University of Tennessee, Knoxville, in 1983. He earned M.S. and Ph.D. degrees in Electrical Engineering from University of Illinois, Urbana-Champaign, in 1985 and 1988, respectively. He has been with Georgia Tech since 1988, where his teaching and research activities have encompassed both the theory and application of control systems, with a particular emphasis on control of electromechanical systems such as robotic motion systems, electric machine systems and power electronic systems.



## Authors



Brian M. Bole graduated from Florida State University in 2008 with a B.S. in Electrical and Computer Engineering and a B.S. in Applied Mathematics. He received a M.S. degree in Electrical Engineering from Georgia Tech in 2011 and he is currently pursuing Ph.D. His research interests include: failure prognostics, stochastic optimization, and fault adaptive control systems.



Samuel Coogan graduated from the Georgia Institute of Technology with a B.S. in Electrical Engineering in 2010. He is currently pursuing M.S. and Ph.D. degrees in the Electrical Engineering and Computer Sciences Department at the University of California, Berkeley.